Physiological and Molecular Plant Pathology 145 (2026) 103353

Contents lists available at ScienceDirect

Physiological and Molecular Plant Pathology

journal homepage: www.elsevier.com/locate/pmpp

Laser dewetting-induced metal particles and their antimicrobial effects

H.K. Lin [a,*], Min-Yang Chen [a,b], Po-Wei Chang [a], Ya-Zhen Xu [b], Ying-Hong Lin [b,**]

[a] Department of Materials Engineering, National Pingtung University of Science and Technology, Pingtung, Taiwan
[b] Department Department of Plant Medicine, National Pingtung University of Science and Technology, Pingtung, 912, Taiwan

ARTICLE INFO

Keywords:
AgCuAl
Guava scab disease
Laser dewetting
Metal-based antifungal agents

ABSTRACT

Guava (*Psidium guajava* L.) is a commercially important tropical fruit widely grown in Asia and South America. However, it is highly susceptible to guava scab disease caused by *Pestalotiopsis psidii*. In Taiwan, the legally approved fungicide, Iminoctadine tris (albesilate), poses significant ecological risks because of its high aquatic toxicity. Therefore, alternative antifungal strategies that warrant further efficacy and safety evaluation are required. This study investigated the antifungal potential of Cu, Ag, AgCu, and AgCuAl nanoparticles prepared by the laser dewetting of sputtered metal films. The antifungal efficacy of the various nanoparticles was evaluated through laboratory and fruit inoculation assays, targeting fungal colony formation, spore germination, germ tube elongation, lesion development, and cellular metabolic activity. Among all tested materials, AgCuAl nanoparticles exhibited the most potent and consistent antifungal performance. They achieved nearly 98–100% inhibition of colony formation, showed complete suppression of spore germination, and produced over 95% reduction in germ tube elongation. Fruit inoculation experiments further demonstrated that AgCuAl almost entirely prevented lesion development, indicating strong protective capability under near-field conditions. Cellular metabolic activity, a key indicator of fungal energy metabolism, was also markedly reduced by approximately 70–80%, confirming substantial disruption of essential cellular functions. In comparison, Ag and AgCu nanoparticles produced moderate inhibition (roughly 40–60%), while Cu nanoparticles led to only minimal suppression (<20%). Overall, these findings confirm the potential of metal nanoparticles, particularly AgCuAl, as a potential alternative antifungal strategy for guava disease management, while further field-relevant validation and safety assessment are needed.

1. Introduction

Guava fruit scab, caused by *Pestalotiopsis psidii*, is a common and damaging disease affecting guava production. The pathogen infects the fruit through natural openings or wounds and causes lesions that severely reduce the commercial value of the fruit [1]. Guava is an economically important fruit crop in Taiwan, with regulated production schedules that allow year-round harvesting. The annual production value of guava fruit is estimated to be 6–7 billion NTD. According to the Ministry of Agriculture, Taiwan, the total cultivation area of guava reached 7797 ha in 2023, with a production volume of 184,504 metric tons. Taiwan cultivates various guava varieties, including 'Zhenzhu Ba' (Pearl guava), 'Zhongshan Yue Ba,' 'Bai Ba,' 'Lizi Ba,' 'Thai Ba,' 'Seedless Ba,' and 'Diwang Ba.' Among these, 'Zhenzhu Ba' is one of the most widely cultivated due to its thick flesh, high sweetness, and balanced acidity. However, this variety is particularly susceptible to guava fruit scab, making it a major concern in Taiwan [2]. Currently, chemical fungicides are the primary means of controlling guava fruit scab (Rao et al., 2012). In Taiwan, the only approved fungicide for managing this disease is Iminoctadine tris (albesilate). However, this chemical poses significant toxicity risks to aquatic organisms [3], and its prolonged application may contribute to the development of fungicide resistance in the pathogen. These concerns highlight the need for safer and more sustainable disease management strategies.

Nanoscale elements exhibit many unique properties compared to their bulk counterparts, owing to their small size and large surface area. Consequently, nanotechnology has been widely applied across various fields, including medicine, biology, physics, chemistry, materials science, electronics, energy, and environmental science. In clinical medicine, nanoparticle technology enhances drug absorption and bioavailability [4–6]. While nanomaterials have been widely explored in biomedical research due to their tunable surface reactivity and

* Corresponding author.
** Corresponding author.
E-mail addresses: HKLin@mail.npust.edu.tw (H.K. Lin), pmyhlin@mail.npust.edu.tw (Y.-H. Lin).

https://doi.org/10.1016/j.pmpp.2026.103353
Received 2 May 2026; Received in revised form 20 June 2026; Accepted 21 June 2026
Available online 23 June 2026

interactions at biological interfaces, these same attributes have also drawn growing interest in sustainable agriculture. In agricultural settings, nanotechnology may improve the precision and efficiency of fertilizer and pesticide delivery, which could help reduce the overuse of conventional agrochemicals. For example, nanosilver (Ag) particles have been investigated as carriers for active ingredients through surface adsorption, potentially enabling lower-dose and sustained-release delivery and thereby improving application efficiency. [7]. Compared with conventional nanoparticle synthesis methods [7–9], the laser dewetting approach offers several advantages, including a more uniform spherical shape [10], higher purity [11], and precisely controllable processing conditions [12]. Compared with conventional wet-chemical syntheses, which often rely on stabilizing agents and can produce colloids that are susceptible to aggregation, laser dewetting converts thin films into substrate-anchored nanoparticles without the use of chemical reducing agents. This approach can offer tunable control over particle size, spacing, and morphology through adjustments in film thickness and laser-processing parameters, while generating immobilized nanostructures that are relatively free of solution-phase contaminants. Such substrate-bound architectures may influence surface wetting and spore–surface interactions, and could therefore contribute to differences in antifungal performance.

Numerous studies have reported that metal-based nanomaterials—including silver (Ag), copper (Cu), and aluminum oxide (Al_2O_3)—can exert inhibitory effects on fungal growth, spore development, and disease progression in a range of plant–pathogen systems [7,13–16]. For instance, laser-dewetted Ag particles (≈1.2 μm) have been reported to achieve complete inhibition of *Colletotrichum gloeosporioides* conidial growth after 5 min of contact [13]. In another study, green-synthesized Cu nanoparticles showed strong activity against *C. capsici*, with CuNP-M at 1000 ppm achieving 99.78% mycelial inhibition, outperforming carbendazim 50 WP at 500 ppm (72.82%) and copper oxychloride 50 WP at 2500 ppm (85.85%) [14]. In addition, biosynthesized Ag nanoparticles have been reported to enhance the antifungal activity of fluconazole against several fungi, including *Phoma glomerata*, *Trichoderma* sp., and *Candida albicans* [15]. Metal alloys combine the properties of multiple metal constituents, which frequently improves both the stability and the antimicrobial performance of the individual metals. Moreover, by adjusting the alloy composition, it is possible to reduce the synthesis cost of expensive metal nanoparticles without compromising their antimicrobial efficacy [17]. For instance, antimicrobial studies conducted by Taner et al. and Zhou et al. revealed that incorporating Cu ions into Ag NPs resulted in the formation of AgCu alloys with enhanced antimicrobial activity. Compared to the individual use of Ag or Cu NPs, AgCu alloys more effectively inhibit the viability of *Escherichia coli* [13,14], thereby demonstrating their potential as effective and economically viable alternatives for pathogen control.

Beyond binary alloys, a study by Wang et al. (2022) demonstrated that high-entropy alloys (HEAs), such as AgCuAl, CuAlZn, and CuAlV, also exhibit excellent thermal stability and corrosion resistance while displaying significant antimicrobial effects against human pathogens. This suggests their potential applicability in a broader range of antimicrobial contexts. The superior microfungal performance of HEAs can be attributed to many factors, including the possible contribution of multiple metal ions, enhanced surface reactivity due to lattice distortion, and sustained ion release that prolongs antifungal activity [15]. Metal- and alloy-based nanoparticles have been reported to suppress phytopathogens through multiple, potentially concurrent pathways, including metal-ion release (e.g., Ag^+ and Cu^{2+}), induction of oxidative stress, and impairment of membrane integrity that can result in leakage of intracellular macromolecules. In addition, contact-mediated interactions between nanostructured surfaces and fungal propagules may inhibit spore germination and early hyphal development [16]. For multi-metal systems, combined surface reactivity and the presence of multiple ionic species have been proposed to contribute to enhanced antifungal activity relative to single-metal controls, although the relative importance of these factors is likely system- and context-dependent.

Given the limitations of currently approved fungicides in Taiwan, this study evaluates the antifungal potential of four nanoparticle systems—Cu, Ag, AgCu, and AgCuAl—prepared by laser dewetting of sputtered metal films. Antifungal activity was assessed using a combination of laboratory assays and controlled fruit inoculation tests. Under the conditions examined, AgCuAl nanoparticles showed the most consistent inhibitory effects across endpoints, including suppression of spore germination and germ tube elongation, reduced lesion development on guava fruit, and a marked decrease in AlamarBlue reduction, indicative of reduced overall cellular metabolic (reducing) activity.

2. Materials and methods

2.1. Films and nanoparticles

Ag, Cu, AgCu, and AgCuAl films with a thickness of 10 nm were deposited on glass substrates using a high-vacuum co-sputtering system equipped with pure Ag, Cu, and Al targets. The sputtering chamber was maintained at a base pressure of 3×10^{-3} Torr, and the flow rate of the working gas (argon) was set to 30 sccm. The film thicknesses were measured using an alpha-step profiler (D-300, KLA-Tencor Co., Ltd., USA). The crystalline phases and structures of the as-deposited films were characterized using X-ray diffraction (XRD) with Cu Kα radiation, operating at 40 mA and 40 kV (Bruker Co., Ltd., USA). The film compositions were confirmed by energy-dispersive X-ray spectroscopy (EDS) using an X-Max detector (Oxford Instruments, UK) at room temperature.

The as-deposited films were dewetted to produce metal NPs using a pulsed near-infrared fiber laser system (SPI Co., Ltd., UK) with a central wavelength of 1064 nm and a laser spot size of 40 μm. The laser processing parameters were optimized using Making Mate software (Eastern Logic Inc., Taipei, Taiwan). The optimal conditions were as follows: repetition frequency: 100 kHz, average laser power: 25 W, scanning speed: 1000 mm/s, and scanning pitch: 20 μm. The surface morphologies of the dewetted films were observed at 50,000× magnification using field-emission scanning electron microscopy (FE-SEM) (Japan Electron Optics Laboratory Co., Ltd., Japan). Static water contact angles were measured using a contact-angle measuring system (OCA-15EC, DataPhysics Instruments GmbH, Germany) at room temperature. A 3 μL droplet of deionized water was deposited on each surface. After laser dewetting process, the surface becomes hydrophilic and the contact angle is 35°.

2.2. Preparation of guava scab pathogen

Strain PM-SSH-081 of guava scab pathogen (*P. psidii*) was isolated by the PM210 Laboratory at Pingtung University of Science and Technology in Taiwan. The terminal hyphae of the pure strain were excised and cultured in potato dextrose agar (PDA) medium (20% potato extract, 2% agar, and 2% dextrose) for subsequent experiments.

2.3. Antifungal tests

The conidia of *P. psidii* were harvested using sterile water and filtered through a 400-mesh stainless steel sieve to remove any mycelial fragments. A conidial suspension was prepared at a concentration of 1×10^3 spores/mL. 150 μL of this suspension was deposited onto thin metal films (glass served as the control). After contact durations of 1, 5, 10, 15, and 30 min, 100 μL of the suspension was retrieved and evenly spread onto PDA medium. The plates were incubated at 28 °C for 24 h, and the colony formation was observed and recorded. The inhibition rate (%) was calculated using the following formula:

$$[(CK - \text{treatment} / CK)] \times 100$$

where *CK* is the number of colonies on the glass control, and *Treatment*

refers to the number of conidia on the metal films (as-deposited or dewetted).

2.4. Spore germination assays

The spore germination rate serves as an important indicator of the inhibitory effects of antifungal agents on pathogen germination. The conidia of *P. psidii* were harvested using sterile water and filtered through a 400-mesh stainless steel sieve to remove any mycelial fragments. A conidial suspension was then prepared at a concentration of 1×10^4 spores/mL. A 150 μL aliquot of the suspension was exposed to the metal NPs for 15 min. Subsequently, four 10 μL droplets of the treated suspension were placed on glass slides, maintained under humid conditions, and incubated in the dark. Spore germination was observed at 0, 4, 8, 12, and 24 h using an optical microscope (OM).

2.5. Inhibition of germ tube elongation

The effects of the various metal NPs on the germ tube development of the pathogen were evaluated by observing the elongation of germ tubes from the conidia over time. Briefly, conidia of *P. psidii* were washed with sterile water and filtered through a 400-mesh stainless steel sieve to remove hyphal fragments. A conidial suspension with a concentration of 1×10^4 spores/mL was prepared. A 150 μL of this suspension was exposed to the test materials for 15 min. After exposure, four 10 μL droplets of the suspension were placed on glass slides and incubated in a moist and dark environment. Germ tube development was observed at 0, 4, 8, 12, and 24 h using an OM.

2.6. Virulence assays

To determine the effects of the metal NPs on the pathogenicity of *P. psidii* conidia, guava fruits were surface-sterilized with 75% ethanol, wiped dry with sterile paper towels, and placed inside a laminar flow hood. A conidial suspension of *P. psidii* was prepared at a concentration of 1×10^4 spores/mL, and a 150 μL aliquot of the suspension was exposed to the metal NPs for 15 min.

The sterilized guava fruits were punctured at three locations with a sterile needle, creating wounds approximately 1 mm deep. A 10 μL droplet of the treated conidial suspension was inoculated into each wound site. Mock samples were included as a negative control by inoculating fruits with sterile water. To maintain humidity, a piece of water agar (WA) medium was placed over each inoculated site, and the fruits were sealed with parafilm. The inoculated fruits were incubated in a growth chamber at 28 °C for two days. After incubation, the WA medium and parafilm were removed, and the diameters of the resulting lesions were measured. Photographs were taken for further analysis.

2.7. AlamarBlue assays

The cellular metabolic activity of *P. psidii* conidia following exposure to metal NPs was evaluated using AlamarBlue Cell Viability Assay (Geno Technology, Inc, USA). Conidia were first washed with sterile water, and a suspension was prepared at a concentration of 1×10^4 spores/mL. A 150 μL aliquot of this suspension was then exposed to the NPs for 15 min. Following exposure, 50 μL of the treated suspension was mixed with 50 μL of potato dextrose broth (PDB) and incubated under gentle shaking for one day.

After incubation, 90 μL of the culture was transferred to a new well, and 10 μL of AlamarBlue dye was added. The mixture was incubated at 28 °C for a further 24 h to allow staining. After staining, the absorbance was measured at 570 and 600 nm using a spectrophotometer (Spectrostar Nano, Germany). The reduction rate of AlamarBlue, which reflects the cellular metabolic activity, was calculated using the following equation, where a higher reduction rate indicates a greater cellular metabolic activity within the conidia:

$$\text{Reduction of AlamarBlue } (\%) = (O2 \times A1) - (O1 \times A2) \times 100 \div (R1 \times N2) - (R2 \times N1)$$

where:

O1: molar absorptivity coefficient of oxidized AlamarBlue at 570 nm (80586)

O2: molar absorptivity coefficient of oxidized AlamarBlue at 600 nm (117216)

R1: molar absorptivity coefficient of reduced AlamarBlue at 570 nm (155677)

R2: molar absorptivity coefficient of reduced AlamarBlue at 600 nm (14652)

A1: absorbance value of test sample at 570 nm.

A2: absorbance value of test sample at 600 nm.

N1: absorbance value of negative control at 570 nm.

N2: absorbance value of negative control at 600 nm.

For data that were approximately normally distributed, results from all assays are reported as mean ± standard deviation (SD). Each treatment was performed using three independent biological replicates ($n = 3$), and all statistical analyses were based on these replicates. One-way analysis of variance (ANOVA) was used to assess statistical differences among groups. When significant differences were detected ($p < 0.05$), all pairwise multiple comparisons were performed using Tukey's Honestly Significant Difference (HSD) test [18]. All statistical analyses were performed using SPSS software (version 20; IBM, Armonk, NY, USA).

3. Results and discussion

3.1. Morphological observation and size analysis of nanoparticles

The particle morphologies of the dewetted samples exhibited clear differences depending on their metal composition. For instance, the Cu and Ag NPs exhibited relatively high circularity, with most of the particles having uniform spherical or ellipsoidal shapes (Fig. 1(a) and (b)). In contrast, the AgCu and AgCuAl particles demonstrated a greater degree of morphological irregularity (Fig. 1(c) and (d)), with many of them having a block-like, clustered, or island-shaped appearance, indicating incomplete or localized dewetting. Despite the morphological differences among the samples [19], the particle size distribution remained relatively consistent, with all the diameters ranging from 90 to 180 nm. The nanoparticle sizes observed in the present experiment are consistent with this result [20], indicating that the laser energy input in our study is sufficient to induce thin-film dewetting and produce nanoparticles of comparable size. Overall, the results suggest that although the composition influences the shape and uniformity of the particles, the size of the particles is determined mainly by the film thickness and laser parameters used in the dewetting process. These observations provide important insights into how the alloy composition affects the NP formation mechanisms, which may in turn influence their functional properties, such as the antifungal activity and surface reactivity.

Although AgCuAl particles exhibit a more irregular, island-like morphology, such nanostructures may increase surface heterogeneity and local defect density, which could enhance interfacial reactivity. In addition, clustered or island-like architectures may influence wetting behavior and spore–surface contact probability during short exposure periods, potentially contributing to the relatively rapid inhibition observed for AgCuAl at early contact times. In the present work an Al-only laser-dewetted control was not included; therefore, the specific contribution of Al cannot be isolated from other compositional and morphological factors in the AgCuAl system. Accordingly, the superior performance of AgCuAl strictly as an observed outcome under the conditions tested, and we frame mechanistic explanations as hypotheses that require further validation.

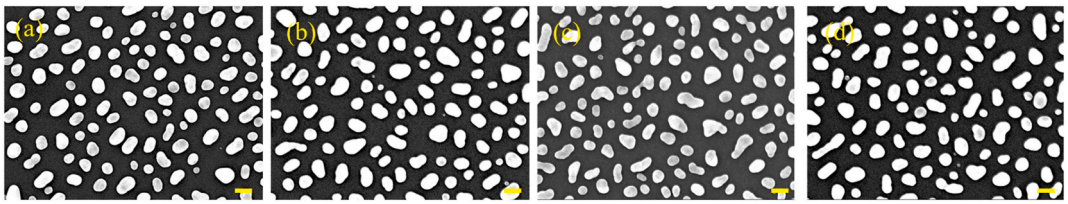

Fig. 1. Scanning electron microscopy (SEM) images of Cu (copper), Ag (silver), AgCu, and AgCuAl particles at 50,000× magnification. (a) Cu nanoparticles, (b) Ag nanoparticles, (c) AgCu nanoparticles, and (d) AgCuAl nanoparticles. The films were deposited onto glass substrates using physical vapor deposition (PVD) sputtering and co-sputtering, and the particles were prepared by dewetting the films using pulsed laser ablation. (Scale bar = 100 nm).

3.2. Antifungal tests

After 1 min of contact between the conidial suspension and the metal particles, Cu showed no detectable inhibition, suggesting minimal antifungal activity at this early stage. In contrast, Ag and AgCu exhibited inhibition rates of 15.8% and 7.6%, respectively. AgCuAl showed a higher inhibition rate (43.1%), which was significantly greater than the other treatments based on the multiple-comparison results in Table 1.

A clear time-dependent increase in inhibition was observed with longer contact durations. After 5 min, Cu still showed limited inhibitory activity, whereas AgCu and Ag reached inhibition rates of 35.1% and 44.0%, respectively. AgCuAl exhibited a markedly higher inhibition rate (86.3%), consistent with the statistical groupings reported in Table 1. At 10 min, Cu showed modest inhibition (11.8%), while AgCu and Ag increased to 58.1% and 77.9%, respectively. AgCuAl reached 99.8% inhibition, indicating near-complete suppression of colony formation. After 15 min, Ag, AgCu, and AgCuAl achieved high inhibition rates (99.3%, 90.2%, and 100%, respectively), whereas Cu remained less effective (23.3%). After 30 min, Ag and AgCuAl both achieved complete inhibition (100%), and AgCu reached 98.8%, while Cu showed 31.7% inhibition (Fig. 2; Table 1). Overall, these results indicate a consistent time-dependent antifungal effect across materials. Under the conditions tested, AgCuAl showed the most rapid and reproducible inhibition, reaching near-complete suppression by 10 min and complete inhibition by 15 min, whereas Cu exhibited comparatively limited activity throughout the assay.

3.3. Spore germination assay

In the glass control group, conidial germination was first detected at 4 h, with 14.3% of conidia forming germ tubes. Germination increased over time, exceeding 50% by 8 h and reaching 89.3% at 48 h, indicating robust germination under the untreated condition. Exposure to Cu particles appeared to partially delay germination. The germination rate at 4 h (13.2%) was comparable to the glass control, but germination progressed more slowly thereafter, reaching ~50% at 24 h and 55.2% at 48 h. Consistent with the multiple-comparison results in Fig. 4, the 48 h germination rate in the Cu treatment was lower than that of the glass control, suggesting a modest inhibitory effect under the conditions tested. Ag and AgCu particles showed greater suppression of germination than Cu. At 4 h, germination rates were 5.3% and 6.5% in the Ag and AgCu groups, respectively. At 48 h, germination remained limited to 29.6% (Ag) and 33.5% (AgCu), indicating stronger inhibition relative to the Cu treatment in this assay.

AgCuAl particles yielded the lowest germination rates throughout the observation period. Germination was 2.3% at 4 h and 15.6% at 48 h, and the 48 h value was lower than those of the other treatments according to the statistical groupings in Fig. 4. Overall, these results suggest that AgCuAl provided the most sustained suppression of conidial germination among the tested materials (Figs. 3 and 4).

3.4. Inhibition of germ tube elongation

In the glass control group, germ tube elongation progressed rapidly. The mean germ tube length reached 7.5 μm at 4 h and 16.2 μm at 8 h, and continued to increase throughout incubation, reaching 105.6 μm at 48 h, indicating active hyphal development in the absence of metal particle exposure. Cu particles appeared to partially suppress germ tube elongation. The mean germ tube length was 7.1 μm at 8 h, increasing to 15.2 μm at 12 h and 36.1 μm at 24 h. By 48 h, the mean germ tube length reached 77.3 μm, which was lower than that of the glass control according to the statistical comparisons shown in Fig. 5, suggesting a modest inhibitory effect under the conditions tested. Ag and AgCu particles showed stronger inhibition of germ tube elongation than Cu. At 12 h, the mean germ tube length in both groups was 6.5 μm. At 24 h, germ tube lengths remained limited to 14.3 μm (Ag) and 13.5 μm (AgCu), indicating greater suppression of germ tube development relative to the Cu treatment. AgCuAl produced the shortest germ tubes among the tested materials. Even after 48 h, only a small proportion of conidia germinated, and the mean germ tube length was 1.0 μm. Consistent with the multiple-comparison results in Fig. 5, the AgCuAl treatment resulted in significantly reduced germ tube elongation relative to the other treatments. This trend is consistent with the colony formation and spore germination assays, supporting the strong inhibitory activity observed for AgCuAl under the experimental conditions (Figs. 3 and 5).

Table 1
Inhibition rates of *Pestalotiopsis psidii* spore suspensions after contact with dewetted Cu, Ag, Al, AgCu, and AgCuAl films for different durations. Spore suspensions (150 μL) were applied to dewetted surfaces and incubated for specified time intervals (1, 5, 10, 15, and 30 min). The treated suspensions were then transferred to PDA plates and cultured at 28 °C. The inhibition rate was determined by comparing the colony formation on dewetted surfaces with that on the untreated control glass surface.

Treatment	Contact time with the film (min)				
	1	5	10	15	30
Glass	-	-	-	-	-
Cu	0.0 ± 0.0 c	0.0 ± 0.0 d	11.8 ± 8.5 c	23.3 ± 8.7 b	31.7 ± 10.8 b
Ag	15.8 ± 7.3 b	44.0 ± 16.4 b	77.9 ± 13.0 a	99.3 ± 0.8 a	100 ± 0.0 a
AgCu	7.6 ± 13.0 b	35.1 ± 11.0 c	58.1 ± 13.4 b	90.2 ± 5.9 a	98.8 ± 0.7 a
AgCuAl	43.1 ± 5.7 a	86.3 ± 3.5 a	99.8 ± 0.8 a	100 ± 0.0 a	100 ± 0.0 a

Data represent mean ± standard deviation (n = 3). Different letters denote statistically significant differences among treatments based on Tukey's HSD test ($p < 0.05$).

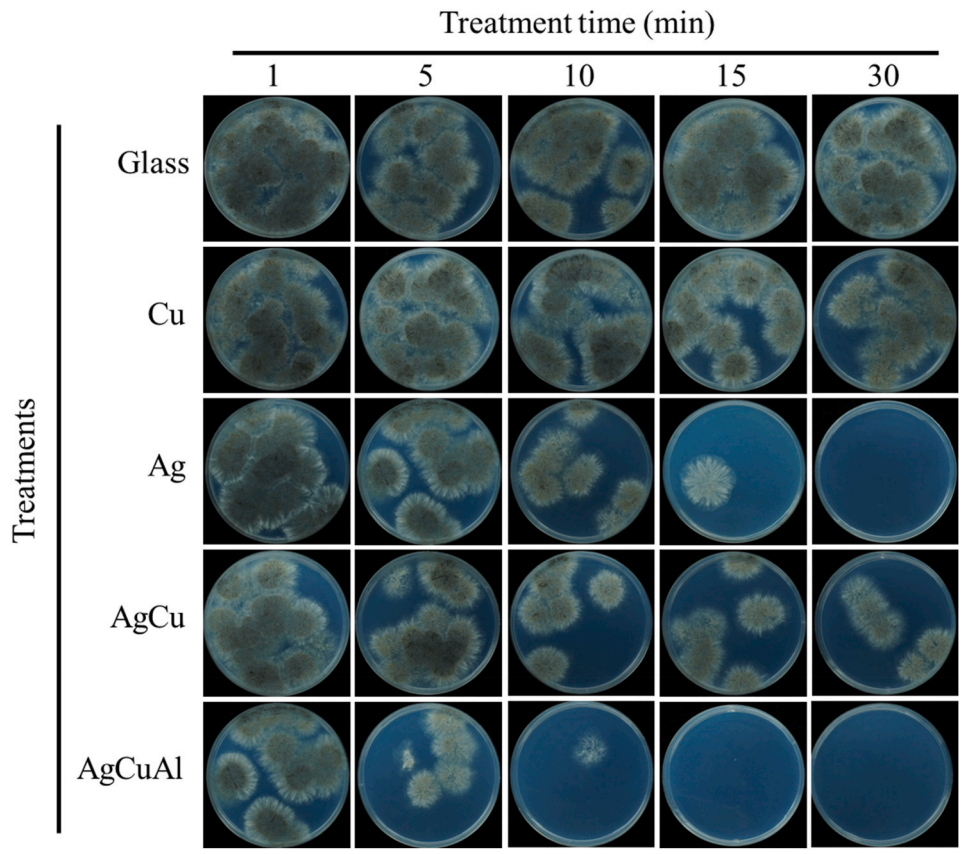

Fig. 2. Photographs of plate colonies formed by *Pestalotiopsis psidii* spore suspensions after contact with dewetted Cu, Ag, AgCu, and AgCuAl films for different durations. Metal films (10 nm) were deposited on glass substrates by sputtering or co-sputtering using pure metal targets. Nanoparticles were produced via laser dewetting using a pulsed fiber laser (1064 nm, 25 W, 100 kHz). Spore suspensions (150 μL) were applied to each surface and incubated for specific contact times before being transferred to PDA plates for colony development.

3.5. Virulence assays

The virulence assay was conducted under controlled fruit inoculation conditions. Each experiment was independently repeated three times, and three fruits were used per treatment in each replicate. Lesion-size measurements and the corresponding statistical comparisons among treatments are summarized in Table 2, which corresponds to the representative fruit inoculation results shown in Fig. 6. In the glass control group, lesion expansion progressed steadily over time. The initial symptoms became visible by day 2, and on day 5, the lesion diameter increased to approximately 23.86 mm. Thus, infection and fungal colonization were unimpeded in the absence of inhibitory treatment. Lesion development was notably suppressed in the fruits inoculated with conidia previously treated with Cu nanoparticles. A gradual increase in the lesion size was observed between days 2 and 5, with the lesion diameter reaching a mean value of 12.26 mm by day 5. This value was significantly lower than that of the control group, thereby demonstrating a moderate in vivo antifungal activity of the Cu-based materials.

The fruits inoculated with conidia treated with Ag and AgCu NPs showed a more pronounced inhibition of lesion formation. By day 5, the average lesion diameters were 4.89 mm for Ag and 5.78 mm for AgCu. Although both treatments significantly reduced disease development compared with the control, there was no significant difference in the lesion size among the Cu, Ag, and AgCu treatments. In other words, all three treatments provided similar levels of partial protection. In fruits inoculated with conidia pre-treated with AgCuAl nanoparticles, no visible lesions were observed by day 5. This suggests that AgCuAl pre-treatment suppressed lesion development under the controlled fruit inoculation conditions used in this study. Together with the in vitro assays, these results indicate that AgCuAl showed the most consistent inhibitory performance across colony formation, spore germination, germ tube elongation, and lesion development endpoints (Fig. 6; Table 2). Nevertheless, because the fruit assay was conducted under controlled conditions, additional work—including field-relevant evaluations and phytotoxicity assessments on host tissues—will be necessary to determine practical applicability and safety under cultivation conditions.

3.6. AlamarBlue assays

Conidia exposed to the glass control exhibited the highest level of cellular metabolic activity, with a dye reduction rate of 81.2%. This high level of cellular metabolic activity was confirmed by the visible color change of the dye from blue to red, which indicated an active and intact cellular metabolic function.

Among the metal-treated groups, the conidia exposed to Cu, Ag, and AgCu NPs showed lower levels of cellular metabolic activity. The differences among the three treatments were not statistically significant, with reduction rates of 38.9% for Cu, 22.0% for AgCu, and 9.5% for Ag. This pattern suggested that the Cu-treated conidia retained the highest level of cellular function, followed by AgCu and Ag. The color of the dye in the Cu treatment changed to purple, indicating partial reduction. Oussou-Azo et al. [21] reported that only high concentrations of Cu-NPs (500 mg/mL) significantly inhibited fungal cell activity and AlamarBlue reduction, while other copper forms showed little effect. Overall, copper materials exhibited moderate antifungal activity, likely mediated through cell membrane damage or metabolic interference rather than direct disruption of cellular function. However, a less intense color change was observed in the AgCu and Ag samples, indicating a reduced cellular function in the two treatments.

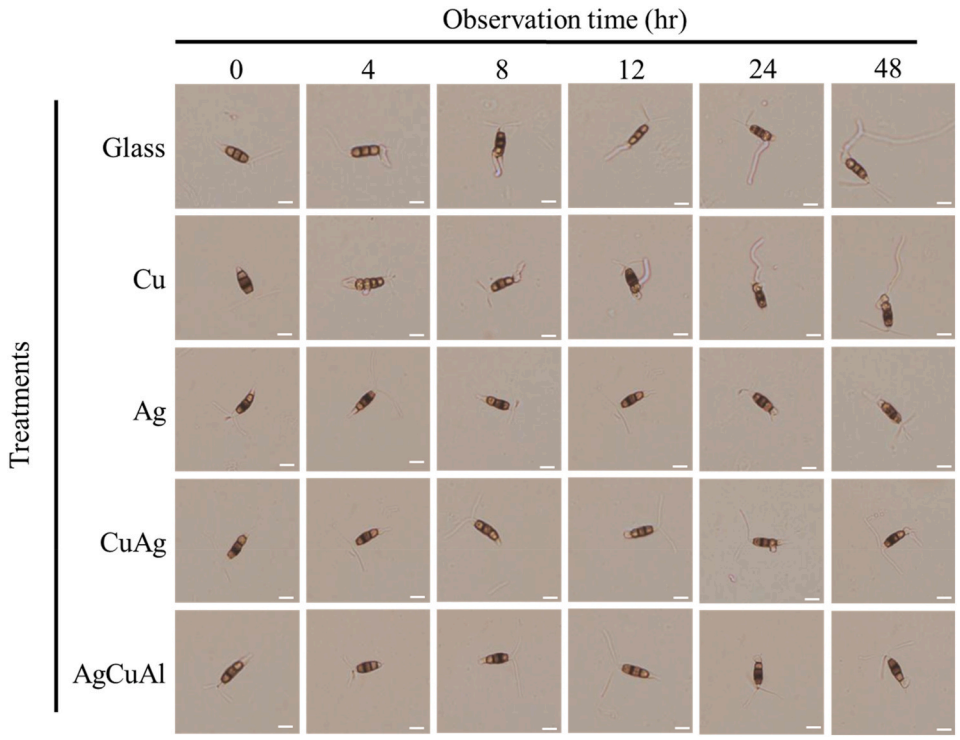

Fig. 3. Microscopic images showing spore germination of *Pestalotiopsis psidii* after 15 min of contact with dewetted Cu, Ag, AgCu, and AgCuAl films (scale bar = 10 μm). Metal films (10 nm) were deposited on glass substrates by sputtering or co-sputtering using pure metal and alloy targets. Nanoparticles were produced via laser dewetting using a pulsed fiber laser (1064 nm, 25 W, 100 kHz). A 150 μL spore suspension was applied to each surface and incubated for 15 min before being transferred for microscopic observation.

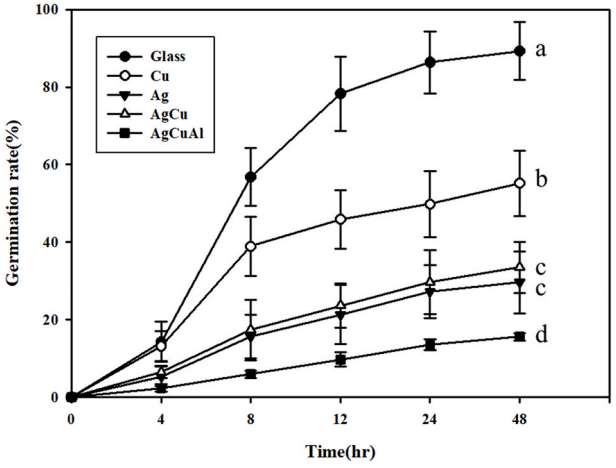

Fig. 4. Spore germination rate of *Pestalotiopsis psidii* after 15-min contact with dewetted Cu, Ag, AgCu, and AgCuAl films, observed over 0–48 h incubation period. Metal films (10 nm) were deposited on glass substrates by sputtering or co-sputtering using pure and alloy targets. Nanoparticles were prepared via laser dewetting using a pulsed fiber laser (1064 nm, 25 W, 100 kHz). A 150 μL spore suspension was applied to each film and allowed to interact for 15 min. Samples were then transferred to fresh medium and incubated under controlled conditions. The germination rate was evaluated microscopically at selected time points between 0 and 48 h. Data represent mean ± standard deviation (n = 3). Different letters denote statistically significant differences among treatments based on Tukey's HSD test ($p < 0.05$).

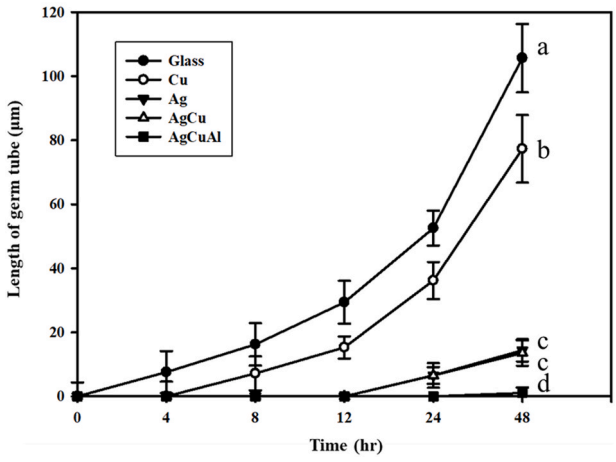

Fig. 5. Germ tube elongation of *Pestalotiopsis psidii* conidia after 15-min contact with dewetted Cu, Ag, AgCu, and AgCuAl films, observed over a 0–48 h incubation period. Metal films with a thickness of 10 nm were deposited on glass substrates via sputtering or co-sputtering using corresponding pure or alloy targets. Nanoparticles were produced by laser dewetting using a pulsed fiber laser (wavelength 1064 nm, power 25 W, repetition rate 100 kHz). A 150 μL spore suspension was dropped onto each dewetted surface and allowed to interact for 15 min. The samples were then transferred to growth medium and incubated under controlled conditions. The germ tube length was measured microscopically at multiple time points between 0 and 48 h. Data represent mean ± standard deviation (n = 3). Different letters denote statistically significant differences among treatments based on Tukey's HSD test ($p < 0.05$).

The AgCuAl-treated conidia exhibited the lowest cellular reducing activity, with an AlamarBlue reduction rate of 3.3%. This value was lower than those of the control, Cu, and AgCu groups according to the statistical comparisons shown in Fig. 7. Consistent with the quantitative result, the AlamarBlue reagent showed no obvious color shift and remained predominantly blue, indicating limited dye reduction. Collectively, these observations suggest that AgCuAl exposure substantially suppressed overall cellular metabolic (reducing) activity in *P. psidii*

Table 2
Lesion size on guava fruit inoculated with *Pestalotiopsis psidii* spore suspensions after contact with Cu, Ag, Al, AgCu, and AgCuAl films and particles. Spore suspensions (150 μL) were exposed to each material for 15 min prior to inoculation. Lesion diameters were measured at the indicated time points after incubation at 28 °C. Mock samples were included as a negative control by inoculating fruits with sterile water.

Treatment	Lesion Size (mm)				
	Day 1	Day 2	Day 3	Day 4	Day 5
Glass	0.00 ± 0.00 a	11.62 ± 1.41 a	13.47 ± 0.80 a	18.84 ± 3.16 a	23.86 ± 2.78 a
Cu	0.00 ± 0.00 a	6.76 ± 1.37 b	9.91 ± 0.51 a	11.10 ± 0.35 b	12.26 ± 1.49 b
Ag	0.00 ± 0.00 a	2.18 ± 0.86 c	3.51 ± 2.28 b	3.86 ± 2.28 bc	4.89 ± 2.30 bc
AgCu	0.00 ± 0.00 a	2.39 ± 2.07 c	3.33 ± 2.96 b	4.64 ± 4.03 c	5.78 ± 5.03 bc
AgCuAl	0.00 ± 0.00 a	0.00 ± 0.00 c	0.00 ± 0.00 b	0.00 ± 0.00 c	0.00 ± 0.00 c
Mock	-	-	-	-	-

Data represent mean ± standard deviation (n = 3). Different letters denote statistically significant differences among treatments based on Tukey's HSD test ($p < 0.05$).

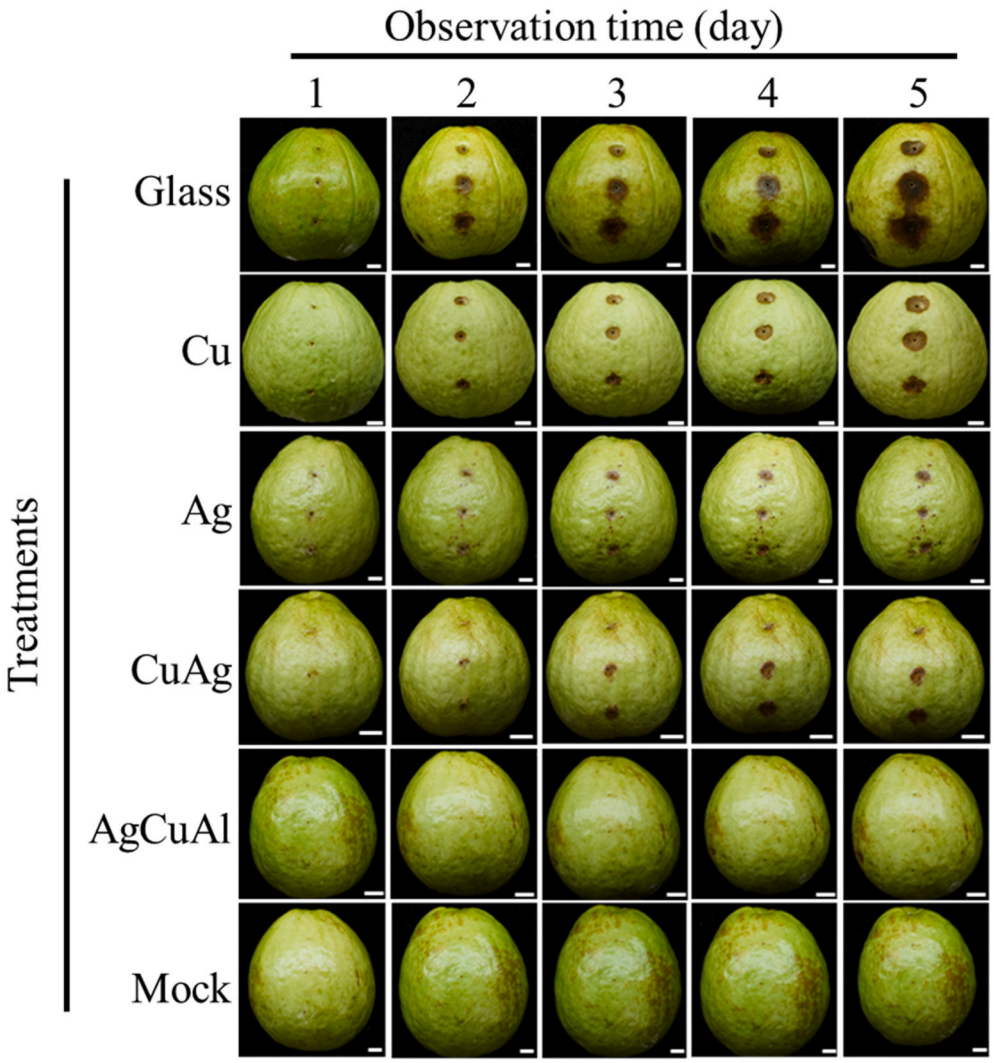

Fig. 6. Lesion development on guava fruit after inoculation with *Pestalotiopsis psidii* spore suspensions previously contacted with dewetted Cu, Ag, AgCu, and AgCuAl films and particles. Spore suspensions (150 μL) were dropped onto the dewetted surfaces and incubated for 15 min. The treated suspensions were then used to inoculate surface-sterilized guava fruits. All the samples were incubated at 28 °C under controlled humidity for 5 days. Mock sample: fruits inoculated with sterile water as a negative control. (Scale bar = 1 cm).

conidia under the experimental conditions (Fig. 7).

To place the antifungal performance of the present AgCuAl system in context, we briefly compare our findings with previously reported nanoparticle-based approaches against phytopathogens. For example, laser-dewetted Ag particles have been reported to inhibit conidial growth of *Colletotrichum gloeosporioides* within short contact periods, supporting the potential relevance of substrate-bound metallic nanostructures for contact-based antifungal applications [13]. In addition, Cu-, Ag-, and Zn-based nanoparticles have been evaluated against a variety of foliar and soil-borne fungal pathogens, suggesting that metal-based nanomaterials can inhibit phytopathogens under certain conditions [22]. More recently, Ag/Cu nanoparticle systems have also been explored for fungal pathogen control, indicating that multi-metal formulations may, in some cases, provide enhanced antifungal

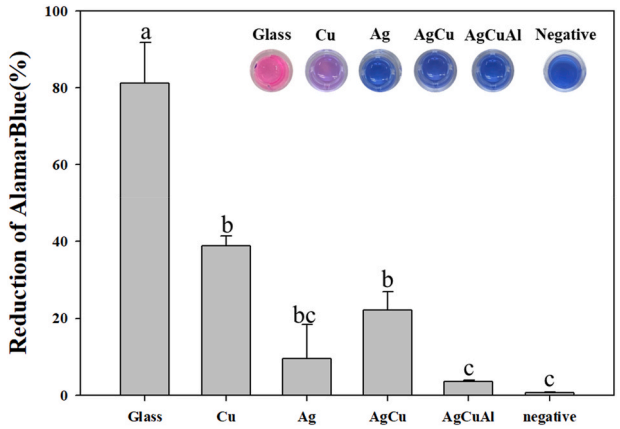

Fig. 7. AmarBlue reduction assay results for *Pestalotiopsis psidii* spore suspensions after contact with dewetted Cu, Ag, AgCu, and AgCuAl films. Spore suspensions (150 μL) were applied to the surfaces of the dewetted films and incubated for 15 min. After contact, the suspensions were transferred to a 96-well plate containing AlamarBlue reagent and incubated at 28 °C for 24 h. The reduction rate of the dye, indicating cellular metabolic (reducing) activity, was calculated based on the absorbance readings obtained using a microplate spectrophotometer at 570 and 600 nm. Negative sample: heat-inactivated spore suspension used as a non-viable control. Data represent mean ± standard deviation (n = 3). Different letters denote statistically significant differences among treatments based on Tukey's HSD test ($p < 0.05$).

performance [18]. In comparison with these reports, the laser-dewetted AgCuAl nanostructures evaluated here showed rapid inhibition within minutes and consistent suppression across multiple endpoints, including colony formation, spore germination, germ tube elongation, and lesion development in a controlled fruit assay. Nevertheless, additional benchmarking using standardized dose–response designs, multiple pathogen isolates, appropriate fungicide comparators, and field-relevant validation will be required to assess robustness and practical applicability.

The consistently strong antifungal activity observed for AgCuAl may be related to the combined effects of multi-metal surface reactivity and heterogeneous interfacial microenvironments associated with ternary alloy nanostructures. Relative to monometallic systems, multi-component alloys can exhibit localized electrochemical heterogeneity, which could influence metal-associated interactions at the spore–surface interface and potentially promote oxidative or membrane-associated damage processes. However, because metal ion release, ROS generation, membrane integrity biomarkers, oxidative stress indicators, and nanoparticle stability in aqueous media were not directly quantified in this study, these mechanistic considerations should be regarded as plausible hypotheses rather than confirmed pathways.

4. Conclusion

This study investigated the antifungal efficacy of Cu, Ag, AgCu, and AgCuAl NPs against *P. psidii* in guava fruit through a series of complementary assays, including tests for colony formation, spore germination, germ tube extension, lesion development, and cellular metabolic activity. Among the materials tested, the AgCuAl NPs consistently demonstrated the strongest inhibitory effect across every assay.

In short-duration contact tests, the AgCuAl particles exhibited notable activity as early as 1 min after exposure and achieved complete inhibition by the 15-min mark. The Ag and AgCu particles also showed high levels of inhibition. However, they required more time to approach full effectiveness. In contrast, the Cu particles displayed a limited antifungal capacity throughout the testing period.

The spore germination and germ tube elongation assays further supported the comparatively strong inhibitory performance of AgCuAl nanoparticles, as this treatment consistently resulted in the lowest germination rates and the shortest germ tube lengths among the tested groups. A similar trend was observed in the controlled fruit inoculation assay: conidia pre-treated with AgCuAl produced no visible lesions by day 5, whereas the other metal-treated groups showed varying degrees of lesion development. At the cellular level, the AlamarBlue assay indicated that AgCuAl treatment was associated with markedly reduced cellular reducing (metabolic) activity in *P. psidii* conidia, as reflected by the lowest dye reduction rate and minimal observable color change (Fig. 7).

Taken together, these results suggest that AgCuAl nanoparticles provided the most consistent antifungal effects across spore germination, germ tube elongation, lesion development, and cellular activity endpoints under the controlled experimental conditions evaluated in this study. Because metal-ion release and intracellular ROS levels were not directly quantified, the basis for the enhanced activity of AgCuAl cannot be definitively resolved here. Nevertheless, the observed performance may reflect multiple contributing factors. Prior studies have shown that Ag^{+} can disrupt membrane integrity and interfere with enzyme function, whereas Cu^{2+} can participate in redox processes that have been linked to oxidative stress. In multi-component alloy systems, the presence of Al may further influence surface chemical states and ion transport behavior, potentially affecting the magnitude and persistence of metal-associated stress responses. Accordingly, the reduced AlamarBlue signal observed after AgCuAl exposure may be consistent with combined effects involving membrane-associated damage, redox imbalance, and impaired cellular metabolism; however, these interpretations remain hypothetical.

Overall, the results of this study suggest that AgCuAl nanoparticles exhibited strong antifungal activity under the experimental conditions tested, including suppression of fungal growth and reduced lesion development in the controlled fruit inoculation assay. In addition, the AlamarBlue assay showed a marked decrease in cellular reducing (metabolic) activity following AgCuAl exposure; however, this endpoint alone does not demonstrate mitochondria-specific damage. Taken together, these findings indicate that AgCuAl is a promising candidate for further development as an antifungal strategy and may offer a potential approach for managing *P. psidii*–associated guava scab, pending validation under field-relevant conditions and further assessment of safety and mechanism.

A key limitation of the present work is that an Al-only laser-dewetted control was not included; therefore, the specific contribution of Al cannot be isolated from other compositional and morphological factors in the AgCuAl system. Accordingly, we present the superior performance of AgCuAl strictly as an observed outcome under the conditions tested, and we frame mechanistic explanations as hypotheses that require further validation.

CRediT authorship contribution statement

H.K. Lin: Conceptualization, Funding acquisition, Project administration, Supervision, Writing – original draft, Writing – review & editing. **Min-Yang Chen:** Conceptualization, Data curation, Formal analysis, Investigation, Methodology, Writing – original draft. **Po-Wei Chang:** Data curation, Formal analysis, Investigation, Visualization. **Ya-Zhen Xu:** Data curation, Formal analysis, Investigation. **Ying-Hong Lin:** Conceptualization, Formal analysis, Investigation, Writing – original draft.

Declaration of competing interest

The authors declare that they have no known competing financial interests or personal relationships that could have appeared to influence the work reported in this paper.

Acknowledgements

The authors gratefully acknowledge the financial support provided to this study by the National Science and Technology Council, ROC, under Project No. NSTC 114-2221-E-020-016.

Data availability

Data will be made available on request.

References

[1] F. Solarte, C.G. Muñoz, S.S. Maharachchikumbura, E. Álvarez, Diversity of Neopestalotiopsis and Pestalotiopsis spp., causal agents of guava scab in Colombia, Plant Dis. 102 (1) (2018) 49–59.
[2] L.M. Keith, M.E. Velasquez, F.T. Zee, Identification and characterization of pestalotiopsis spp. causing scab disease of guava, Psidium guajava, in Hawaii, Plant Dis. 90 (1) (2006) 16–23.
[3] V.I. Lushchak, T.M. Matviishyn, V.V. Husak, J.M. Storey, K.B. Storey, Pesticide toxicity: a mechanistic approach, Excli j 17 (2018) 1101–1136.
[4] H. Chhipa, Chapter 6 - applications of nanotechnology in agriculture, in: V. Gurtler, A.S. Ball, S. Soni (Eds.), Methods in Microbiology, Academic Press, 2019, pp. 115–142.
[5] S.E. McNeil, Nanotechnology for the biologist, J. Leukoc. Biol. 78 (3) (2005) 585–594.
[6] S. Potharaju, Z.A. Jaaz, Development and characterization of antimicrobial nanocoatings for titanium dental implants to prevent peri-implantitis and improve osseointegration, SHIFAA 2023 (2023) 10–18.
[7] S. Kaabipour, S. Hemmati, A review on the green and sustainable synthesis of silver nanoparticles and one-dimensional silver nanostructures, Beilstein J. Nanotechnol. 12 (2021) 102–136.
[8] A. Nyabadza, É. McCarthy, M. Makhesana, S. Heidarinassab, A. Plouze, M. Vazquez, D. Brabazon, A review of physical, chemical and biological synthesis methods of bimetallic nanoparticles and applications in sensing, water treatment, biomedicine, catalysis and hydrogen storage, Adv. Colloid Interface Sci. 321 (2023) 103010.
[9] F. Ruffino, M.G. Grimaldi, Nanostructuration of thin metal films by pulsed laser irradiations: a review 9 (8) (2019) 1133.
[10] C.A. Horwood, E. Owusu-Ansah, Y.J. Shi, V.I. Birss, Pulsed laser induced dewetting of Au thin films on Ta2O5 substrates, Chem. Phys. 541 (2021) 110926.
[11] S.Z. Mat Isa, R. Zainon, M. Tamal, State of the art in gold nanoparticle synthesisation via pulsed laser ablation in liquid and its characterisation for molecular imaging: a review, Materials 15 (3) (2022) 875.
[12] J. Yu, J. Nan, H. Zeng, Size control of nanoparticles by multiple-pulse laser ablation, Appl. Surf. Sci. 402 (2017) 330–335.
[13] F. Zhou, Y. Zhu, L. Yang, D.-Q. Yang, E. Sacher, Ag NP catalysis of Cu ions in the preparation of AgCu NPs and the mechanism of their enhanced antibacterial efficacy, Colloids Surf. Physicochem. Eng. Aspects 632 (2022) 127831.
[14] M. Taner, N. Sayar, I.G. Yulug, S. Suzer, Synthesis, characterization and antibacterial investigation of silver–copper nanoalloys, J. Mater. Chem. 21 (35) (2011) 13150–13154.
[15] J.J. Wang, H.K. Lin, W.S. Chuang, C.Y. Chuang, Y.-H. Lin, J.C. Huang, Y.-H. Lin, Laser dewetting mechanism and antibacterial properties of Cu-Al based medium entropy alloy films, J. Alloys Compd. 903 (2022) 163893.
[16] S.M. Ouda, Antifungal activity of silver and copper nanoparticles on two plant pathogens, Alternaria alternata and Botrytis cinerea, Res. J. Microbiol. 9 (1) (2014) 34–42.
[17] K.-H. Huynh, X.-H. Pham, J. Kim, S.H. Lee, H. Chang, W.-Y. Rho, B.-H. Jun, Synthesis, properties, and biological applications of metallic alloy nanoparticles, Int. J. Mol. Sci. 21 (14) (2020) 5174.
[18] I.S. Lopes, J.K.C. Soares, L.S. de Medeiros, L. Coronato Courrol, Evaluation of ALA-capped silver, copper, and silver–copper nanoparticles for controlling fungal plant pathogens, Microb. Pathog. 191 (2024) 106672.
[19] Z.A. Hussein, Z.A. Talib, Study the bacterial resistance of antibiotic from opportunistic bacteria, SHIFAA 2024 (2024) 63–79.
[20] H.K. Lin, I.C. Chen, W.H. Lu, J.Y. Cheng, J.J. Wang, Laser-induced silver nanoparticles with HfO2 shell for melamine detection, Sensor Actuator Phys. 364 (2023) 114789.
[21] A.F. Oussou-Azo, T. Nakama, M. Nakamura, T. Futagami, M.d.C.M. Vestergaard, Antifungal potential of nanostructured crystalline copper and its oxide forms, Nanomaterials 10 (5) (2020) 1003.
[22] A.A. Malandrakis, N. Kavroulakis, C.V. Chrysikopoulos, Use of copper, silver and zinc nanoparticles against foliar and soil-borne plant pathogens, Sci. Total Environ. 670 (2019) 292–299.